



**Tin and Germanium Based Two-dimensional  
Ruddlesden–Popper Hybrid Perovskites for Potential  
Lead–Free Photovoltaic and Photoelectronic Applications**

Journal:	<i>Nanoscale</i>
Manuscript ID	NR-COM-05-2018-003589.R1
Article Type:	Communication
Date Submitted by the Author:	30-May-2018
Complete List of Authors:	Ma, Liang; University of Nebraska-Lincoln, Chemistry Ju, Minggang; University of Nebraska-Lincoln, Department of Chemistry Dai, Jun; University of Nebraska-Lincoln, Chemistry Zeng, Xiao Cheng; University of Nebraska-Lincoln, Department of Chemistry



Journal Name

ARTICLE

## Tin and Germanium Based Two-dimensional Ruddlesden–Popper Hybrid Perovskites for Potential Lead–Free Photovoltaic and Photoelectronic Applications†

Received 00th January 20xx,  
Accepted 00th January 20xx

DOI: 10.1039/x0xx00000x

www.rsc.org/

Liang Ma,<sup>a</sup> Ming-Gang Ju,<sup>a</sup> Jun Dai<sup>a</sup> and Xiao Cheng Zeng<sup>\*a,b</sup>

Despite of their high power conversion efficiency the commercial applications of the hybrid organic-inorganic lead (Pb) halide perovskite based solar cells are still hampered by concern of element Pb toxicity and the structural stability in open air. Herein, based on density-functional theory computation, we show that the lead-free tin (Sn) and germanium (Ge)-based two-dimensional (2D) Ruddlesden-Popper hybrid organic-inorganic perovskites with few-unit-cell thickness,  $\text{BA}_2\text{MA}_{n-1}\text{M}_n\text{I}_{3n+1}$  ( $\text{M}=\text{Sn}, \text{Ge}, n=2-4$ ), possess desirable electronic, excitonic and light absorption properties, thereby promising for photovoltaic and/or photoelectronic applications. In particular, we show that by increasing the layer thickness of the Sn-based 2D perovskites, the bandgap can be lowered towards the optimal range (0.9–1.6 eV) for solar cells. Meanwhile, the exciton binding energy is reduced to a more optimal value. In addition, theoretical assessment indicates that the thermodynamic stability of Sn-/Ge-based 2D perovskites is notably enhanced compared to their 3D analogue. These features render the Sn-/Ge-based 2D hybrid perovskites with a few tens of unit cells in thickness a promising lead-free perovskites with much improved structural stabilities for photovoltaic and/or photoelectronic applications.

Hybrid organic-inorganic lead (Pb) halide perovskites, commonly refer as to the methylammonium (MA:  $\text{CH}_3\text{NH}_3^+$ ) lead iodide ( $\text{MAPbI}_3$ ) or formamidinium (FA:  $\text{NH}_2\text{CH}=\text{NH}_2^+$ ) lead iodide ( $\text{FAPbI}_3$ ), have been broadly recognized as a promising candidate for the next-generation cost-effective solar cells, whose power conversion efficiency (PCE) has reached as high as ~22.1%.<sup>1, 2</sup> Despite of their high PCE, the poor open-air stability of the bulk  $\text{MAPbI}_3/\text{FAPbI}_3$  perovskite remains to be a challenge prior to large-scale commercial applications.<sup>3</sup> The use of toxic Pb element in the  $\text{MAPbI}_3/\text{FAPbI}_3$  based solar cells is also of environment and health concerns.<sup>4, 5</sup>

Numerous strategies have been proposed to resolve the instability issue of the hybrid perovskites, such as changing or mixing halide ions and/or organic cations, altering the electron and/or hole transport materials (ETM/HTM) or modifying additives of ETM/HTM.<sup>6</sup> Recent studies suggested that by inserting bulky alkylammonium cations, e.g., butylammonium (BA:  $\text{C}_4\text{H}_9\text{NH}_3^+$ ) or phenylethylammonium (PEA:  $\text{C}_8\text{H}_9\text{NH}_3^+$ ), three-dimensional (3D)  $\text{MAPbI}_3$  can be sliced into 2D Ruddlesden-Popper form with a general formula of  $\text{A}_2\text{MA}_{n-1}\text{Pb}_n\text{I}_{3n+1}$  ( $\text{A}=\text{PEA}, \text{BA}, \text{etc}$ ). Previous experiments showed that the 2D Ruddlesden-Popper hybrid perovskites exhibit highly

enhanced moisture stability, compared to the 3D analogue, due to the protective organic ligand layer made of PEA or BA.<sup>7-14</sup> The planar structures of 2D hybrid perovskites enable efficient encapsulation which further improves the open-air stability. Besides the improved stability, the 2D Ruddlesden-Popper  $\text{A}_2\text{MA}_{n-1}\text{Pb}_n\text{I}_{3n+1}$  perovskites with high  $n$  values ( $n \geq 3$ ) are quite promising for PSC device with rapid increase of PCE from initial 4.02–4.79%<sup>8, 9</sup> to 12.5%.<sup>11</sup> Recently, a certified PCE of 15.3% for  $\text{PEA}_2\text{MA}_{n-1}\text{Pb}_n\text{I}_{3n+1}$  with  $n=60$  is reported along with highly improved device performance longevity.<sup>10</sup>

Meanwhile, many efforts have been devoted to achieving efficient lead-free perovskites. Strategies reported thus far include replacing all or partial Pb with tin (Sn) or germanium (Ge) or mixed Sn-Ge in the perovskites.<sup>4, 5, 15-17</sup> However, the Ge- and Sn-based hybrid perovskites still entail similar instability issue as both perovskites can be easily oxidized from +2 to +4 valence state, thereby disrupt the initial perovskite structures.<sup>4, 5</sup> To date, few experimental trial has been undertaken for the materials synthesis and device fabrication, which largely impedes the advancement of Sn- and Ge-based PSCs.<sup>5</sup> Another strategy to obtain Pb-free or Pb-less perovskite materials is to synthesize chalcogenide-based perovskites or double perovskites,<sup>18-21</sup> although the PCE values reported thus far are still low.

The much-enhanced stability of 2D Pb-based perovskites motivated this study to examine the properties of Sn- and Ge-based 2D Ruddlesden-Popper hybrid perovskites with reduced dimensionality while improved stability. Note that previous experimental studies already demonstrated the feasibility of

<sup>a</sup> Department of Chemistry and Nebraska Center for Materials and Nanoscience, University of Nebraska–Lincoln, Lincoln, Nebraska 68588, United States. Email: xzeng1@unl.edu

<sup>b</sup> Department of Chemical & Biomolecular Engineering and Department of Mechanical & Materials Engineering, Lincoln, Nebraska 68588, United States.

†Electronic Supplementary Information (ESI) available. See DOI: 10.1039/x0xx00000x

Sn- and Ge-based 2D Ruddlesden-Popper hybrid perovskites about two decades ago.<sup>7, 22, 23</sup> In addition, previous studies suggested

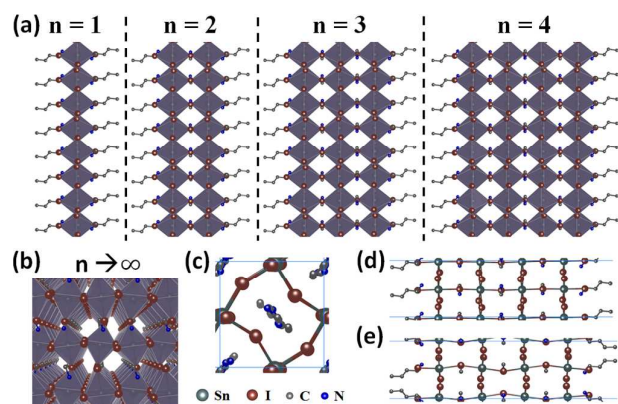


**Fig. 1** (a) Structure schemes of  $\text{BA}_2\text{MA}_{n-1}\text{Sn}_n\text{I}_{3n+1}$  ( $n=1-4$ ) and (b)  $\text{MASnI}_3$  ( $n \rightarrow \infty$ ). Example atomic view of the unit cell of  $\text{BA}_2\text{MA}_3\text{Sn}_4\text{I}_{13}$  ( $n=4$ ) along (c)  $c$ -axis, (d)  $a$ -axis and (e)  $b$ -axis, respectively (all hydrogen atoms are removed for clarity).

that single-unit-cell-thick ( $n=1$ )  $\text{BA}_2\text{SnI}_4$  and  $\text{BA}_2\text{GeI}_4$  can serve as the lead-free 2D hybrid perovskite semiconductors with tunable bandgaps and small effective carrier masses, which renders the  $\text{BA}_2\text{SnI}_4$  and  $\text{BA}_2\text{GeI}_4$  good potentials for photoelectronic applications.<sup>24, 25</sup>

However, as a trade-off of the improved stability, the bandgaps of the thinnest 2D hybrid perovskites,  $\text{BA}_2\text{MI}_4$  ( $M=\text{Ge}, \text{Sn}, \text{Pb}$ ) with single-unit-cell thickness ( $n=1$ ), are much larger than that of bulk  $\text{MAPbI}_3$ , all beyond the optimal range of 0.9–1.6 eV for solar cells.<sup>26</sup> Moreover, their higher exciton binding energies make the separation of photo-excited electron-hole pairs (excitons) harder, due to the quantum confinement effect with the reduced dimensionality.<sup>24</sup> Hence, a natural strategy would be to increase the layer thickness ( $n$ ) of the 2D hybrid perovskites to gain back some properties of their 3D analogues, such as smaller bandgaps, reduced exciton binding energies, as well as improved light absorption, while retaining good stability of the 2D forms.<sup>27</sup>

In this work, we investigate the electronic and excitonic properties of Sn- and Ge- based 2D hybrid perovskites with few-unit-cell thickness,  $\text{BA}_2\text{MA}_{n-1}\text{M}_n\text{I}_{3n+1}$  ( $M=\text{Sn}, \text{Ge}, n=2-4$ ), by using ab initio computation methods. We find that both the bandgaps and exciton binding energies of the 2D hybrid perovskites can be gradually reduced via increasing  $n$  from 2 to 4. We note that very recently, the 2D Sn-based PSCs with  $n=2-6$  have been experimentally fabricated with the PCE of 1.94% (for  $n=3$ ) and 2.53% (for  $n=4$ ).<sup>28</sup> The much thicker ( $n=9$ ) 2D Sn-based PSCs yield the PCE of 5.94% without further device-structure engineering.<sup>29</sup> The latter PCE value is very close to the state-of-the-art value (6.4%), achieved with the lead-free perovskite  $\text{MASnI}_3$ .<sup>30</sup> By mixing the 2D Sn-based perovskites with 3D  $\text{FASnI}_3$ , highly reproducible Sn-based PSCs with 9% PCE is experimentally achieved with much improved stability.<sup>31</sup> Further improvement of the PCE and stability of the 2D Sn-based PSCs is highly anticipated.

The density-functional theory (DFT) calculations were performed with using the Vienna Ab initio Simulation Package (VASP 5.4).<sup>32, 33</sup> The projected augmented wave (PAW) method and the Perdew-Burke-Ernzerhof (PBE) functional within the

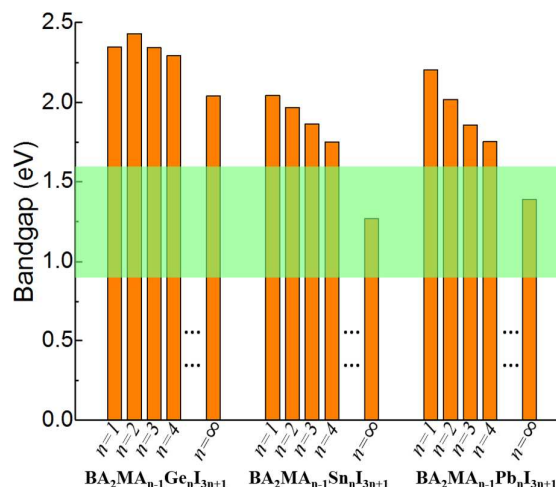


**Fig. 2** Computed electronic bandgap of  $\text{BA}_2\text{MA}_{n-1}\text{M}_n\text{I}_{3n+1}$  ( $M=\text{Ge}, \text{Sn}$  and  $\text{Pb}; n=1-4$  and  $\infty$ ) based on the hybrid functional plus SOC schemes. The light-green horizontal bar denotes the optimal bandgap range (0.9–1.6 eV) for solar cells.

generalized gradient approximation (GGA) were employed.<sup>34-36</sup> The Grimme's DFT-D3 scheme was adopted to describe the dispersion correction.<sup>37</sup> For bandgap computation, the more accurate PBE0<sup>38</sup> hybrid functional were used to obtain the electronic structures of Sn- and Ge-based 2D hybrid perovskites. The spin-orbit coupling (SOC) effect was included in the DFT computations. More computational details can be found in the part I of ESI.

The structure schemes of 2D  $\text{BA}_2\text{MA}_{n-1}\text{Sn}_n\text{I}_{3n+1}$  ( $n=1-4$ ) and 3D  $\beta$ -phase  $\text{MASnI}_3$  ( $n \rightarrow \infty$ ) are presented in Fig. 1(a) and (b), respectively (see ESI Fig. S1 and S2 for the Ge and Pb cases). The lattice constants computed based on the PBE+D3 method are presented in ESI Table S1, whose values are in good agreement with experimental results. These 2D perovskites structures consist of multiple inorganic sheets of corner-sharing  $[\text{MI}_6]^{4-}$  octahedral, terminated by the intercalated bulky BA cations from two opposite surfaces. As the  $[\text{MI}_6]^{4-}$  octahedral sheet number  $n$  increases, the 2D hybrid perovskite structures slowly approach to their corresponding 3D bulk. It is expected that their bandgaps decrease and gradually approach to the value of 3D bulk.

Fig. 2 shows the bandgaps of  $\text{BA}_2\text{MA}_{n-1}\text{Ge}_n\text{I}_{3n+1}$ ,  $\text{BA}_2\text{MA}_{n-1}\text{Sn}_n\text{I}_{3n+1}$  and  $\text{BA}_2\text{MA}_{n-1}\text{Pb}_n\text{I}_{3n+1}$  ( $n=1-4$  and  $\infty$ ) computed by hybrid functional +SOC schemes. Note that the computed bandgaps, 2.04 eV, 1.27 eV and 1.39 eV, are in good agreement with the measured ones, i.e., 1.9–2.0 eV,<sup>17, 39</sup> 1.2–1.3 eV<sup>15, 28, 30</sup> and  $\sim 1.5$  eV,<sup>40</sup> for  $\text{MAGeI}_3$ ,  $\text{MASnI}_3$  and  $\text{MAPbI}_3$ , respectively, which validates our theoretical approach (see part II of ESI). Nearly all the computed bandgaps of 2D hybrid perovskites are reduced by increasing the layer thickness ( $n$ ). The two exceptions are the  $\text{BA}_2\text{GeI}_4$  and  $\text{BA}_2\text{MAGE}_2\text{I}_7$ , with the bandgap of the latter being larger than the former by 0.08 eV.

The difference can be understood by the lattice expansion of  $\text{BA}_2\text{MAGe}_2\text{I}_7$  caused by the MA ion which is absent in  $\text{BA}_2\text{GeI}_4$ . As the atomic radius of Ge (1.25 Å) is less than that of Sn (1.45 Å) and Pb (1.54 Å),<sup>41</sup> the lattice constants of  $\text{BA}_2\text{GeI}_4$  are less than those of  $\text{BA}_2\text{SnI}_4$  and  $\text{BA}_2\text{PbI}_4$  by  $\sim 2\%$ – $3\%$  along  $a$  axis and

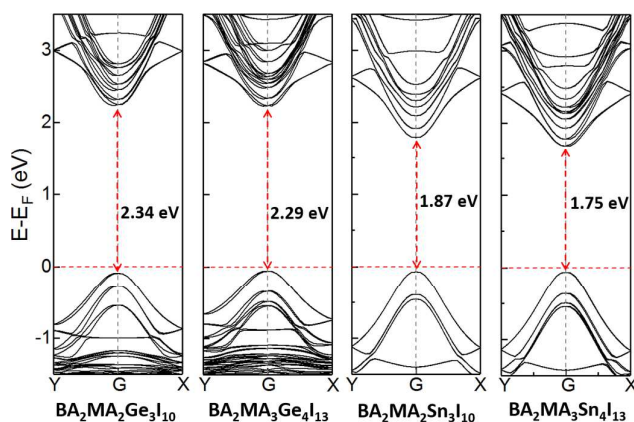


**Fig. 3** Computed band structures of  $\text{BA}_2\text{MA}_{n-1}\text{M}_n\text{I}_{3n+1}$  ( $\text{M}=\text{Ge}, \text{Sn}, n=3-4$ ) based on the PBE0+SOC scheme. The G (0, 0, 0), X (0.5, 0, 0), and Y (0, 0.5, 0) are the high-symmetry special points in the first Brillouin zone. The Fermi level is set to zero.

$\sim 4\%$ – $5\%$  along  $b$  axis (see ESI Table S1), respectively, thereby resulting in smaller interspace between  $[\text{GeI}_6]^{4-}$  octahedrons. From single to double  $[\text{GeI}_6]^{4-}$  octahedral sheets, the lattice constant along  $b$  axis is enlarged by  $\sim 3.6\%$  to accommodate the MA ions, compared with the enlargement of  $\sim 1.7\%$  and  $\sim 1.2\%$  for the Sn and Pb case, respectively. The lattice expansion induced excess strain is responsible for the anomalous bandgap increase from  $\text{BA}_2\text{GeI}_4$  to  $\text{BA}_2\text{MAGe}_2\text{I}_7$ . Beyond the thickness of the latter, the bandgaps of  $\text{BA}_2\text{MA}_{n-1}\text{Ge}_n\text{I}_{3n+1}$  monotonically decrease with increasing of the number of  $[\text{GeI}_6]^{4-}$  octahedral sheets from  $n = 2$  to 4 within the individual layer. As can be seen from Fig. 2, the bandgaps of Sn-based 2D hybrid perovskites decrease monotonically as the increase of  $n$ , eventually approaching the bandgap of 3D  $\text{MASnI}_3$ . The latter bandgap is within the optimal range (0.9–1.6 eV) for solar cells. It is thus reasonably expected that the Sn-based 2D hybrid perovskites with high layer-number ( $n > 4$ ) show optimal bandgaps for solar cell while their stabilities would be superior to their 3D analogues (will be discussed later). Although the bandgaps of Ge-based 2D perovskites are all above the optimal range for solar cells, they could still be used in tandem solar cells to promote open circuit voltage.<sup>39</sup>

As the bandgaps of Sn-based 2D hybrid perovskites ( $n=3-4$ ) are closer to the optimal bandgaps of light absorber materials, the calculated electronic band structures of  $\text{BA}_2\text{MA}_{n-1}\text{Sn}_n\text{I}_{3n+1}$  ( $n = 3-4$ ) are shown in Fig. 3. The  $n = 3-4$  cases of Ge-based 2D hybrid perovskites are also included for comparison (see ESI Fig. S3 for the  $n = 1-2$  cases of Sn- and Ge-based 2D perovskites and Fig. S4 for the Pb case). The 2D hybrid perovskites are all direct-gap semiconductors with the valence band maximum (VBM) and conduction band minimum (CBM) located at the Gamma (G) point. It is known that the carrier (hole and electron) mobility plays a vital role in the

performance of solar cells, a property also closely related to the carrier effective mass. We calculate the effective masses of hole ( $m_h^*$ ) and electron ( $m_e^*$ ), based on the band structures and the formula  $m^* = \hbar^2 / (\partial^2 E / \partial k^2)$ , where  $\hbar$  is the reduced Planck constant,  $k$  is the magnitude of wave vector in momentum space, and  $\partial^2 E / \partial k^2$  is obtained by fitting the energy dispersion curves near the VBM and CBM with simple parabolic function for the hole and electron, respectively. Both hole and electron effective masses increase with the layer thickness  $n$  for the Ge- and Sn-based 2D perovskites (see ESI Tables S5 and S6). As the SOC induced energy band spin splitting also increases with the 2D perovskite thickness, slightly non-parabolic behavior arises from the crossing of sub-band, resulting in the increase of carrier effective mass.<sup>27</sup> Previously, a similar trend has been experimentally observed in the 2D quantum wells of carbon-doped (100)  $\text{GaAs}/\text{Al}_x\text{Ga}_{1-x}\text{As}$  heterostructures, which might be saturated at a critical thickness.<sup>42</sup>

The 2D hybrid perovskites can be viewed as a heterogeneously stacked sandwich structure. The enhanced carrier effective mass for the 2D hybrid perovskites is expected to be saturated at a critical  $n$ . Indeed, we find that the carrier effective masses of  $\text{BA}_2\text{MA}_{n-1}\text{Pb}_n\text{I}_{3n+1}$  increase from  $n = 1-3$  but decrease from  $n = 3-4$  (see ESI Table S7). So we predict that for Pb-based 2D perovskites the critical  $n$  is around  $n = 4$ , consistent with results of a recent study.<sup>43</sup> For the Sn and Ge based 2D perovskites, however, the determination of the critical  $n$  is beyond our current computational capability, thus it calls for future experimental determination. The effective masses of Ge- and Sn-based 2D hybrid perovskites are generally smaller than those of Pb counterparts, implying higher carrier mobility may be expected for the Ge- and Sn-based 2D hybrid perovskites. Likewise, bulk  $\text{MASnI}_3$  has a very high carriers mobility over  $2000 \text{ cm}^2/(\text{V}\cdot\text{s})$ , measured from a previous experiment.<sup>40</sup>

The in-plane Wannier-Mott exciton binding energy ( $E_b$ ) of the 2D hybrid perovskites can be estimated by using a modified hydrogen-atom-like Bohr model as  $E_b = \mu e^4 / 2\hbar^2 \epsilon^2$ ,<sup>44</sup> where  $\epsilon$  is the dielectric constant calculated by the density functional perturbation theory (DFPT),<sup>45</sup>  $\mu = m_e^* \times m_h^* / (m_e^* + m_h^*)$  is the reduced effective mass of exciton (hole-electron pair) and  $e$  is the charge of electron (see ESI Tables S5-S7). As expected,  $E_b$  decreases as increasing thickness  $n$  due to the reduced bandgaps and enhanced dielectric properties for all 2D hybrid perovskites. It is shown that  $E_b$  of Ge- and Sn-based 2D hybrid perovskites are much smaller than that of Pb counterpart, and Sn's case has the smallest  $E_b$  at the same  $n$ . Thus, the separation of photo-excited exciton (electron-hole pair) into free carriers would be easier in Ge- and Sn-based 2D hybrid perovskites than in Pb counterpart. Further reduction of  $E_b$  is highly feasible through increasing  $n$ , rendering thicker ( $n > 4$ ) 2D hybrid perovskites more suitable for photovoltaic and/or photoelectronic applications.

As the sunlight absorption with absorber materials is critical to the performance of solar cell, we compute the absorption properties of the Sn- and Ge-based 2D hybrid perovskites, namely, the absorption coefficient  $\alpha$  based on the formula<sup>46</sup>

$$\alpha = \sqrt{2} \frac{\nu}{c} \left[ \sqrt{\varepsilon_1(\nu)^2 + \varepsilon_2(\nu)^2} - \varepsilon_1(\nu) \right]^{1/2}, \quad (1)$$

where  $\nu$  is the photon frequency,  $c$  is the speed of light in vacuum,  $\varepsilon_1(\nu)$  and  $\varepsilon_2(\nu)$  are the real and imaginary parts of the dielectric function. Note that computation of the absorption spectra based on the PBE0+SOC scheme is extremely expensive due to the need of much denser k-point grid (see part I of ESI). Hence, we calculate the absorption spectra of the 2D hybrid

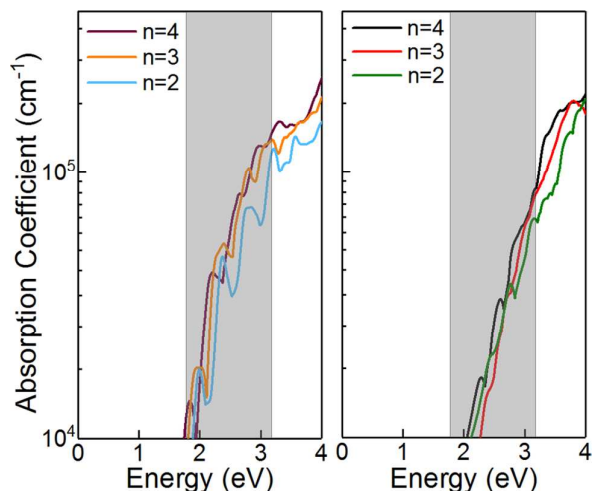
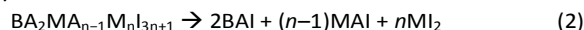


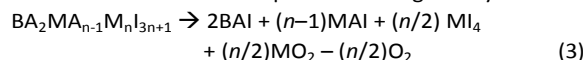
**Fig. 4** Computed light absorption spectra of  $\text{BA}_2\text{MA}_{n-1}\text{Sn}_n\text{I}_{3n+1}$  (left panel) and  $\text{BA}_2\text{MA}_{n-1}\text{Ge}_n\text{I}_{3n+1}$  (right panel) for  $n=2-4$ , respectively. The light-grey vertical bar denotes the photon energy range of visible light (wavelengths in  $\sim 390$  nm–700 nm).

perovskites ( $n=2-4$ ) by using the PBE functional, followed by shifting the absorption peak by  $\Delta_{\text{PBE0}} - \Delta_{\text{PBE}}$  ( $\Delta$ : bandgap). As shown in Fig. 4, the light absorption of Sn- and Ge-based 2D hybrid perovskites over the visible light range can be improved by increasing the layer thickness  $n$ . A similar trend can be seen for the Pb-based 2D hybrid perovskites (see ESI Fig. S5). Therefore, thicker ( $n>4$ ) 2D hybrid perovskites are expected to be more desirable for solar cell device. Moreover, the light absorption of Sn based 2D perovskites is expected to be better than the Ge based 2D perovskites in the visible light range due to the smaller fundamental bandgaps of Sn-based perovskites.

Experimentally, the temporal stability of 2D perovskites are superior to their 3D analogue.<sup>28</sup> This is partially due to the protective organic ligand layer. Nevertheless, a deeper understanding of the improved stability of 2D hybrid perovskites is still required. To this end, we assess the thermodynamic stability of 2D perovskites  $\text{BA}_2\text{MA}_{n-1}\text{M}_n\text{I}_{3n+1}$  ( $\text{M}=\text{Ge}, \text{Sn}, \text{Pb}$ ) by computing the decomposition enthalpy ( $\Delta H_{\text{dec}}$ ), defined as the energy change from the decomposition of the 2D perovskites. Negative  $\Delta H_{\text{dec}}$  means that the decomposition is endothermic and thermodynamically unfavorable, whereas positive  $\Delta H_{\text{dec}}$  means that the decomposition is exothermic and is thermodynamically favorable. One possible pathway (pathway 1) is simply given by<sup>29</sup>



where  $\text{M}=\text{Ge}, \text{Sn}$  and  $\text{Pb}$  and  $n=1-4$  and  $\infty$  (3D). Since the  $\text{Sn}^{2+}/\text{Ge}^{2+}$  can be readily oxidized into  $\text{Sn}^{4+}/\text{Ge}^{4+}$ , another possible decomposition pathway (pathway 2) involving oxygen for the Sn- and Ge-based 2D perovskites is given by



The computed decomposition enthalpy (per metal atom) of the corresponding pathways (1 for Ge, Sn, Pb; and 2 for Ge and Sn) of 2D hybrid perovskites versus thickness  $n$  are presented in Fig. 5 and ESI Table S8. The negative  $\Delta H_{\text{dec}}$  in lower-half of Fig. 5 suggest that the Ge/Sn/Pb-based 2D perovskites are all stable with respect to pathway 1. While the positive  $\Delta H_{\text{dec}}$

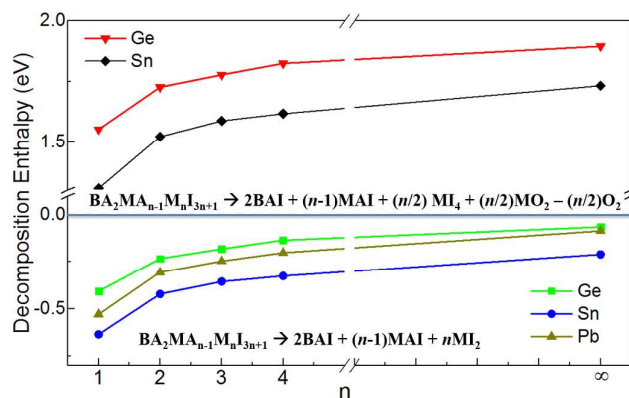


**Fig. 5** The calculated decomposition enthalpy (per metal atom) with respect to two possible pathways (lower-half for pathway 1 and upper-half for pathway 2) of  $\text{BA}_2\text{MA}_{n-1}\text{M}_n\text{I}_{3n+1}$  ( $\text{M}=\text{Ge}, \text{Sn}, \text{Pb}, n=1-4$  and  $\infty$ ). Only +2 valence state of metal ion is considered in the pathway 1 (eq. 2) and no oxygen is involved. While the pathway 2 (eq. 3) is merely based on the  $\text{Sn}^{4+}/\text{Ge}^{4+}$  ions with oxygen involved.

in upper-half of Fig. 5 indicate that the Ge/Sn/Pb-based 2D perovskites are unstable with respect to the pathway 2. The  $\Delta H_{\text{dec}}$  decreases as  $n$  decreases. Hence,  $\Delta H_{\text{dec}}$  for  $n = \infty$  (3D  $\text{MAMI}_3$ ) is the highest; and that for  $n = 1$  is the lowest for both pathways. The positive value of  $\Delta H_{\text{dec}}$  for pathway 2 suggest that the oxidation of Sn- and Ge-based perovskite in air is exothermic, and is thus thermodynamically favourable. While the significant decrease of  $\Delta H_{\text{dec}}$  with the decrease of  $n$  for the pathway 2 implies that the oxidation resistance of Sn- and Ge-based 2D perovskites is higher for smaller  $n$ , similar to the elevated moisture resistance of 2D perovskites, due to the encapsulating organic ligand layer and reduced dimensionality.<sup>8, 29</sup> Also, the positive value of  $\Delta H_{\text{dec}}$  for the pathway 2 with oxygen involved implies that further improved encapsulation technique is critical to the protection of Sn- and Ge-based 2D perovskites from contact with oxygen. The higher members of 2D perovskites ( $n>4$ ) are expected to show less advantage than those  $n=1-4$  cases regarding the thermodynamic stability but could be still superior to their 3D analogue. On the other hand, the efficiency of 2D perovskites solar cells are expected to be promoted as  $n$  increases. Thus, finding the balance between the respectable efficiency and acceptable stability for 2D hybrid perovskites solar cells would be a future direction in 2D perovskite research.

## Conclusions

In conclusion, we have investigated the electronic, excitonic and light-absorption properties of Sn- and Ge-based 2D hybrid perovskites,  $\text{BA}_2\text{MA}_{n-1}\text{M}_n\text{I}_{3n+1}$  ( $\text{M}=\text{Sn}, \text{Ge}, n=2-4$ ), with few-unit-cell thickness. We find that their bandgaps decrease from 2.04 eV to 1.75 eV for Sn-based and from 2.35 eV to 2.29 eV for Ge-based 2D perovskites, respectively, by increasing the layer thickness from  $n=1$  to 4. The bandgaps of Sn-based 2D perovskites approach the optimal bandgap range for solar cells. The smaller carrier effective masses of the Sn- or Ge-based 2D hybrid perovskites imply their carrier mobility may be higher than the Pb counterpart. The exciton binding energies are also reduced while the light absorption is improved with increasing the layer thickness. We expect that Sn- and Ge-based 2D hybrid perovskites with several to tens of unit-cell thickness would exhibit even smaller bandgaps, more reduced exciton binding energy, and better light absorption. In addition, it is found that the thermodynamic stability of 2D perovskites is notably enhanced compared to their 3D analogue. All these features of Sn- and Ge-based 2D perovskites are highly desirable for the design of lead-free hybrid perovskite photovoltaic and/or photoelectronic applications with reasonable performance and greatly enhanced device longevity.

## Conflicts of interest

There are no conflicts to declare.

## Acknowledgements

This work is supported by the National Science Foundation (NSF) through the Nebraska Materials Research Science and Engineering Center (MRSEC) (grant No. DMR-1420645), an NSF EPSCoR Track 2 grant (OIA-1538893), and by the University of Nebraska Holland Computing Center.

## Notes and references

- W. S. Yang, B.-W. Park, E. H. Jung, N. J. Jeon, Y. C. Kim, D. U. Lee, S. S. Shin, J. Seo, E. K. Kim, J. H. Noh and S. I. Seok, *Science*, 2017, **356**, 1376-1379.
- M. L. Petrus, J. Schlipf, C. Li, T. P. Gujar, N. Giesbrecht, P. Müller-Buschbaum, M. Thelakkat, T. Bein, S. Hüttner and P. Docampo, *Adv. Energy Mater.*, 2017, **7**, 1700264.
- N. H. Tiep, Z. Ku and H. J. Fan, *Adv. Energy Mater.*, 2016, **6**, 1501420.
- Z. Shi, J. Guo, Y. Chen, Q. Li, Y. Pan, H. Zhang, Y. Xia and W. Huang, *Adv. Mater.*, 2017, **29**, 1605005.
- M. Lyu, J.-H. Yun, P. Chen, M. Hao and L. Wang, *Adv. Energy Mater.*, 2017, **7**, 1602512.
- J. You, L. Meng, T.-B. Song, T.-F. Guo, Y. Yang, W.-H. Chang, Z. Hong, H. Chen, H. Zhou, Q. Chen, Y. Liu, N. De Marco and Y. Yang, *Nat. Nanotechnol.*, 2016, **11**, 75-81.
- D. B. Mitzi, *Chem. Mater.*, 1996, **8**, 791-800.
- I. C. Smith, E. T. Hoke, D. Solis-Ibarra, M. D. McGehee and H. I. Karunadasa, *Angew. Chem. Int. Ed.*, 2014, **53**, 11232-11235.
- D. H. Cao, C. C. Stoumpos, O. K. Farha, J. T. Hupp and M. G. Kanatzidis, *J. Am. Chem. Soc.*, 2015, **137**, 7843-7850.
- L. N. Quan, M. Yuan, R. Comin, O. Voznyy, E. M. Beauregard, S. Hoogland, A. Buin, A. R. Kirmani, K. Zhao, A. Amassian, D. H. Kim and E. H. Sargent, *J. Am. Chem. Soc.*, 2016, **138**, 2649-2655.
- H. Tsai, W. Nie, J.-C. Blancon, C. C. Stoumpos, R. Asadpour, B. Harutyunyan, A. J. Neukirch, R. Verduzco, J. J. Crochet, S. Tretiak, L. Pedesseau, J. Even, M. A. Alam, G. Gupta, J. Lou, P. M. Ajayan, M. J. Bedzyk, M. G. Kanatzidis and A. D. Mohite, *Nature*, 2016, **536**, 312-316.
- J.-C. Blancon, H. Tsai, W. Nie, C. C. Stoumpos, L. Pedesseau, C. Katan, M. Kepenekian, C. M. M. Soe, K. Appavoo, M. Y. Sfeir, S. Tretiak, P. M. Ajayan, M. G. Kanatzidis, J. Even, J. J. Crochet and A. D. Mohite, *Science*, 2017, **355**, 1288-1292.
- Y. Chen, Y. Sun, J. Peng, J. Tang, K. Zheng and Z. Liang, *Adv. Mater.*, 2017, **30**, 1703487.
- M. Yuan, L. N. Quan, R. Comin, G. Walters, R. Sabatini, O. Voznyy, S. Hoogland, Y. Zhao, E. M. Beauregard, P. Kanjanaboos, Z. Lu, D. H. Kim and E. H. Sargent, *Nat. Nanotechnol.*, 2016, **11**, 872-877.
- F. Hao, C. C. Stoumpos, D. H. Cao, R. P. H. Chang and M. G. Kanatzidis, *Nat. Photonics*, 2014, **8**, 489-494.
- M.-G. Ju, J. Dai, L. Ma and X. C. Zeng, *J. Am. Chem. Soc.*, 2017, **139**, 8038-8043.
- C. C. Stoumpos, L. Frazer, D. J. Clark, Y. S. Kim, S. H. Rhim, A. J. Freeman, J. B. Ketterson, J. I. Jang and M. G. Kanatzidis, *J. Am. Chem. Soc.*, 2015, **137**, 6804-6819.
- M.-G. Ju, J. Dai, L. Ma and X. C. Zeng, *Adv. Energy Mater.*, 2017, **7**, 1700216.
- J. Dai, L. Ma, M. Ju, J. Huang and X. C. Zeng, *Phys. Chem. Chem. Phys.*, 2017, **19**, 21691-21695.
- M.-G. Ju, M. Chen, Y. Zhou, H. F. Garces, J. Dai, L. Ma, N. P. Padture and X. C. Zeng, *ACS Energy Lett.*, 2018, **3**, 297-304.
- M.-G. Ju, M. Chen, Y. Zhou, J. Dai, L. Ma, N. P. Padture and X. C. Zeng, *Joule*, 2018, DOI: 10.1016/j.joule.2018.04.026.
- D. B. Mitzi, C. A. Feild, W. T. A. Harrison and A. M. Guloy, *Nature*, 1994, **369**, 467-469.
- C. R. Kagan, D. B. Mitzi and C. D. Dimitrakopoulos, *Science*, 1999, **286**, 945-947.
- L. Ma, J. Dai and X. C. Zeng, *Adv. Energy Mater.*, 2017, **7**, 1601731.
- M. Pandey, K. W. Jacobsen and K. S. Thygesen, *J. Phys. Chem. Lett.*, 2016, **7**, 4346-4352.
- W. Shockley and H. J. Queisser, *J. Appl. Phys.*, 1961, **32**, 510-519.
- L. Zhang and W. Liang, *J. Phys. Chem. Lett.*, 2017, **8**, 1517-1523.
- D. H. Cao, C. C. Stoumpos, T. Yokoyama, J. L. Logsdon, T.-B. Song, O. K. Farha, M. R. Wasielewski, J. T. Hupp and M. G. Kanatzidis, *ACS Energy Lett.*, 2017, **2**, 982-990.
- Y. Liao, H. Liu, W. Zhou, D. Yang, Y. Shang, Z. Shi, B. Li, X. Jiang, L. Zhang, L. N. Quan, R. Quintero-Bermudez, B. R. Sutherland, Q. Mi, E. H. Sargent and Z. Ning, *J. Am. Chem. Soc.*, 2017, **139**, 6693-6699.
- N. K. Noel, S. D. Stranks, A. Abate, C. Wehrenfennig, S. Guarnera, A.-A. Haghighirad, A. Sadhanala, G. E. Eperon,

## ARTICLE

## Journal Name

- S. K. Pathak, M. B. Johnston, A. Petrozza, L. M. Herz and H. J. Snaith, *Energy Environ. Sci.*, 2014, **7**, 3061-3068.
31. S. Shao, J. Liu, G. Portale, H.-H. Fang, G. R. Blake, G. H. ten Brink, L. J. A. Koster and M. A. Loi, *Adv. Energy Mater.*, 2018, **8**, 1702019.
32. G. Kresse and J. Furthmüller, *Phys. Rev. B*, 1996, **54**, 11169-11186.
33. G. Kresse and J. Furthmüller, *Comput. Mater. Sci.*, 1996, **6**, 15-50.
34. P. E. Blöchl, *Phys. Rev. B*, 1994, **50**, 17953-17979.
35. G. Kresse and D. Joubert, *Phys. Rev. B*, 1999, **59**, 1758-1775.
36. J. P. Perdew, K. Burke and M. Ernzerhof, *Phys. Rev. Lett.*, 1996, **77**, 3865-3868.
37. S. Grimme, J. Antony, S. Ehrlich and H. Krieg, *J. Chem. Phys.*, 2010, **132**, 154104.
38. J. Paier, R. Hirschl, M. Marsman and G. Kresse, *J. Chem. Phys.*, 2005, **122**, 234102.
39. T. Krishnamoorthy, H. Ding, C. Yan, W. L. Leong, T. Baikie, Z. Zhang, M. Sherburne, S. Li, M. Asta, N. Mathews and S. G. Mhaisalkar, *J. Mater. Chem. A*, 2015, **3**, 23829-23832.
40. C. C. Stoumpos, C. D. Malliakas and M. G. Kanatzidis, *Inorg. Chem.*, 2013, **52**, 9019-9038.
41. E. Clementi, D. L. Raimondi and W. P. Reinhardt, *J. Chem. Phys.*, 1967, **47**, 1300-1307.
42. H. Zhu, K. Lai, D. C. Tsui, S. P. Bayrakci, N. P. Ong, M. Manfra, L. Pfeiffer and K. West, *Solid State Commun.*, 2007, **141**, 510-513.
43. C. C. Stoumpos, D. H. Cao, D. J. Clark, J. Young, J. M. Rondinelli, J. I. Jang, J. T. Hupp and M. G. Kanatzidis, *Chem. Mater.*, 2016, **28**, 2852-2867.
44. J. M. Frost, K. T. Butler, F. Brivio, C. H. Hendon, M. van Schilfgaarde and A. Walsh, *Nano Lett.*, 2014, **14**, 2584-2590.
45. S. Baroni, P. Giannozzi and A. Testa, *Phys. Rev. Lett.*, 1987, **58**, 1861-1864.
46. S. Saha, T. P. Sinha and A. Mookerjee, *Phys. Rev. B*, 2000, **62**, 8828-8834.